



HAL
open science

Neuropilin-1 regulates platelet-derived growth factor receptor signaling in mesenchymal stem cells

Stephen G Ball, Christopher Bayley, C Adrian Shuttleworth, Cay M Kielty

► **To cite this version:**

Stephen G Ball, Christopher Bayley, C Adrian Shuttleworth, Cay M Kielty. Neuropilin-1 regulates platelet-derived growth factor receptor signaling in mesenchymal stem cells. *Biochemical Journal*, 2010, 427 (1), pp.29-40. 10.1042/BJ20091512 . hal-00479264

HAL Id: hal-00479264

<https://hal.science/hal-00479264>

Submitted on 30 Apr 2010

HAL is a multi-disciplinary open access archive for the deposit and dissemination of scientific research documents, whether they are published or not. The documents may come from teaching and research institutions in France or abroad, or from public or private research centers.

L'archive ouverte pluridisciplinaire **HAL**, est destinée au dépôt et à la diffusion de documents scientifiques de niveau recherche, publiés ou non, émanant des établissements d'enseignement et de recherche français ou étrangers, des laboratoires publics ou privés.

Neuropilin-1 regulates platelet-derived growth factor receptor signaling in mesenchymal stem cells

Stephen G. Ball, Christopher Bayley, C. Adrian Shuttleworth and Cay M. Kielty*

Wellcome Trust Centre for Cell-Matrix Research, Faculty of Life Sciences, University of Manchester, UK.

Running title: Neuropilin-1 regulates PDGFRs

*Corresponding author:
Cay M Kielty
Faculty of Life Sciences,
University of Manchester,
Michael Smith Building
Oxford Road,
Manchester, M13 9PT.
Tel. +44 161 275 5739
Fax +44 161 275 5082
Email: cay.kielty@manchester.ac.uk

SYNOPSIS

Using human mesenchymal stem cells lacking vascular endothelial growth factor (VEGF) receptors, we show that the pro-angiogenic receptor neuropilin-1 associates with phosphorylated platelet-derived growth factor (PDGF) receptors, thereby regulating cell signaling, migration, proliferation and network assembly. Neuropilin-1 co-immunoprecipitated and co-localized with phosphorylated PDGF receptors in the presence of growth factors. Neuropilin-1 knockdown blocked PDGF-AA-induced PDGF receptor-alpha phosphorylation and migration, reduced PDGF-BB induced PDGF receptor-beta activation and migration, blocked VEGF-A activation of both PDGF receptors, and attenuated proliferation. Neuropilin-1 prominently co-localized with both PDGF receptors within mesenchymal stem cell networks assembled in matrigel and in the chorioallantoic membrane vasculature microenvironment, and its knockdown grossly disrupted network assembly and decreased PDGF receptor signaling. Thus, neuropilin-1 regulates mesenchymal stem cells by forming ligand-specific receptor complexes that direct PDGF receptor signaling, especially the PDGF receptor-alpha homodimer. This receptor crosstalk may control the mobilization of mesenchymal stem cells in neovascularization and tissue remodeling.

KEYWORDS

Co-localization

Mesenchymal stem cells

Migration

Network assembly

Neuropilin-1

Platelet-derived growth factor receptors

ABBREVIATIONS

bFGF, basic fibroblast growth factor

CAM, chorioallantoic membrane

DAPI, 4',6-diamidino-2-phenylindole

HGF, hepatocyte growth factor

HUVEC, human umbilical vein endothelial cell

MSC, mesenchymal stem cell

NRP, neuropilin

PDGF, platelet-derived growth factor

PI3K, phosphoinositide 3-kinase

RFU, relative fluorescent units

RT-PCR, reverse transcription-PCR

Scr, scrambled

siRNA, small interfering RNA

VEGF, vascular endothelial growth factor

INTRODUCTION

Mesenchymal stem cells (MSCs) in bone marrow and perivascular niches throughout the body are reservoirs of multipotent cells that can differentiate along mesenchymal lineages including smooth muscle and undergo endothelial transdifferentiation in response to vascular endothelial growth factor (VEGF) [1-3]. We have shown that multipotent human MSCs express neuropilin-1 (NRP-1) and platelet-derived growth factor (PDGF) receptors (PDGFRs) α and β , but not VEGF receptors (VEGFRs), and that both PDGFs and VEGF-A stimulate PDGFRs thereby regulating proliferation, migration and smooth muscle-specific cytoskeleton [2, 4].

NRP-1 is a type I transmembrane glycoprotein that regulates vascular and neural development and acts as a co-receptor for VEGFRs and plexins [5-11]. NRP-1 deficient or over-expressing mice display severe abnormalities in nervous and cardiovascular systems [12, 13], whilst NRP-1 null zebrafish have loss of circulation via angiogenic vessels [14]. The large extracellular region of NRP-1 comprises two complement binding (CUB) domains (designated a1a2), two coagulation factor V/VIII homology domains (designated b1b2), and a MAM (meprin, A5 antigen, receptor tyrosine phosphatase μ) domain (designated c). The last three C-terminal residues of NRP-1 form a PDZ binding motif that influences NRP-1-mediated angiogenesis [15, 16]. NRP-1 is highly expressed by numerous tumor cell lines, and enhances tumor survival, growth and vascularization *in vivo* [17-19].

In vascular endothelial cells, NRP-1 and VEGFR2 co-cluster but do not interact directly in the absence of VEGF-A₁₆₅ [20, 21]. NRP-1 b1b2 domains can bind the basic C-terminal tail of the heparan sulfate binding growth factor VEGF-A₁₆₅, which bridges extracellularly between VEGFR2 and NRP-1, generating a complex with enhanced VEGFR2 signaling that can

induce angiogenic sprouting [7, 22-26]. Cytoplasmic domains also contribute to VEGFR2/NRP-1 receptor complexes, since inhibiting VEGFR phosphorylation or deleting the PDZ domain of NRP-1 reduces this association [27]. In tumor cells that lack expression of VEGFR2, NRP-1 supports VEGF-mediated endothelial cell migration through PI3K/Akt signaling, implying the existence of other receptors for NRP-1-mediated VEGF function [28, 29]. Indeed, NRP-1 associates with heparan sulfate-binding growth factors bFGF and HGF [30], and can regulate HGF-induced c-met phosphorylation [31]. PDGF-B also influences vascular smooth muscle cell motility by up-regulating and associating with NRP-1 [32].

The PDGFR and VEGFR tyrosine kinases, and their growth factor ligands, are closely related structurally and evolutionarily [33-34]. PDGF growth factors induce receptor-specific activation, with PDGF-AA stimulating only PDGFR α , whereas PDGF-BB stimulates all PDGFR dimers $\alpha\alpha$, $\beta\beta$ and $\alpha\beta$ [35]. PDGF-CC binds to PDGFRs $\alpha\alpha$ and $\alpha\beta$ [35], whilst PDGF-AB mainly signals through PDGFR $\alpha\beta$ [36]. In early embryonic development, PDGFR α and its major ligand PDGF-A are co-expressed from the two-cell stage, and PDGF-A stimulated PDGFR α signaling is critical for differentiation of ES cells to mesenchymal, neural crest, cranial cells and myogenic cells, and for epithelial-mesenchymal transformation [37-39]. PDGF-A knockout is embryonic lethal, PDGFR α null mice die during embryonic development, and mice null for PDGF-C die perinatally [34, 40]. PDGFRs are also essential regulators of vessel wall development [41] and remodeling following injury [42], with PDGF-B a major mitogenic and chemotactic ligand for smooth muscle cells and their mesenchymal precursors. NRP-1 expression also identifies vascular precursors in embryonic stem cells [43].

It was recently shown that bone marrow cells are recruited to sites of neovascularization through NRP-1 [44]. Here, using MSCs lacking VEGFRs, we show that NRP-1 co-

localization with phosphorylated PDGFRs, regulates their signaling in a ligand-specific manner, and has an indispensable role in PDGFR α induced migration and MSC network assembly. This novel receptor crosstalk may thus control the recruitment of MSCs in vascular remodeling.

Accepted Manuscript

THIS IS NOT THE VERSION OF RECORD - see doi:10.1042/BJ20091512

EXPERIMENTAL

Cell culture and reagents

Human MSCs from normal bone marrow of 20 and 26 year old females and 18, 22 and 24 year old males (obtained from Lonza), were cultured on 0.1% gelatine (Sigma-Aldrich) and maintained and characterized as described previously [45]. For each analysis, MSCs were analyzed at passage 4. HUVECs from 35 and 29 year old females (Cascade Biologics) were maintained as described previously [45]. All growth factors were obtained from R&D Systems and VEGFR2 tyrosine kinase inhibitor V was supplied by MERK.

Flow cytometry

For single-color flow cytometry, MSCs (4×10^6 cells/ml) were incubated with either PE-conjugated anti-human neuropilin-1 (FAB3870P), VEGFR2 (FAB357P) or control anti-IgG₁ (IC002P) (R&D Systems), then processed as previously described [2].

Immunofluorescence microscopy

MSCs were cultured on round glass coverslips in 24-well culture dishes, previously coated with 0.1% gelatin overnight at 4°C, or a thin-layer of growth factor reduced Matrigel (BD Biosciences) incubated at 37°C for 30 min. Cells were fixed with 4% (w/v) paraformaldehyde for 20 min, incubated in 0.2 M glycine for 20 min, then permeabilized using 0.5% Triton X-100 (w/v) in PBS for 4 min. After blocking in 2% fish skin gelatin in PBS (Sigma-Aldrich), pairs of primary antibodies in blocking solution were incubated overnight at 4°C. Primary antibodies were all obtained from Santa Cruz; anti-human NRP-1 (sc-5541), NRP-1 (sc-7239), p-PDGFR α -Y754 (sc-12911), p-PDGFR α -Y720 (sc-12910), PDGFR α (sc-338), p-PDGFR β -Y1021 (sc-12909-R), p-PDGFR β -Y751 (sc-21902-R), p-Flk-1-Y1175 (sc-101819) and PDGFR β (sc-339). Cells were then incubated with appropriate Alexa-488 and Alexa-555

fluorophores (Invitrogen) in blocking solution for 2 h at room temperature and coverslips mounted onto glass slides with ProLong Gold antifade reagent with DAPI (Invitrogen). Images were collected on a Nikon C1 confocal using a TE2000 PSF inverted microscope, utilizing 60× /NA 1.40 Plan Apo or 20× /NA 0.50 Plan Fluor objectives and 3× confocal zoom. Different sample images detecting the same antibodies were acquired under constant acquisition settings. Images were processed using Nikon EZ-C1 FreeViewer v3.3 software. For co-localization analysis, images were processed using ImageJ software and co-localization analysis plugin. For each analyzed image, similar best-fit lower threshold values were determined to reduce signal background of the corresponding red and green channels, then particle sizes for the red and green channels set at a minimum of 1 pixel and maximum of 1000 pixels, then co-localization between channels determined and represented by a yellow image.

Migration and proliferation assays

MSC migration was determined utilizing a modified Boyden chamber assay as previously described [2]. The number of migratory MSCs on the membrane underside (cells/field using a 10× /NA 0.3 UPlan F1 objective) were determined using an Olympus BX51 widefield microscope. Images were captured with a CoolSNAP camera system and processed using MetaMorph imaging v5.0 software. To determine proliferation, MSCs (2,000 cells/well) in growth medium were seeded in 96-well plates coated with 0.1% gelatin and incubated with or without PDGF ligands at 37°C, with growth medium and ligands exchanged every 24 h. At the end of each time point, a CyQuant cell proliferation assay kit (Invitrogen) was utilized to detect MSC proliferation as previously described [2].

siRNA transfections

MSCs (5×10^5 cells) together with $3 \mu\text{g}$ small interfering RNAs (siRNA) were transfected by electroporation using a human Nucleofector kit (Amaxa), then cultured for 20 h in growth medium at 37°C in a humidified atmosphere of 5% CO_2 in air. Two different validated siRNAs, functionally tested to provide $\geq 70\%$ target gene knockdown for neuropilin-1 were obtained from (i) Qiagen (S102663213) and (ii) Ambion (4390824) and a scrambled siRNA control (Qiagen). The targeting specificity and efficiency following individual siRNA knockdowns was evaluated using primers and RT-PCR analysis, as previously described [2,45].

Immunoprecipitation analysis

MSC lysates were isolated as previously described [45], then $100 \mu\text{g}$ lysate incubated with anti-human neuropilin-1 (sc-7239), PDGFR α (sc-338) or PDGFR β (sc-339) (Santa Cruz) overnight at 4°C . Immune complexes were isolated by incubation with 10% (w/v) protein A-Sepharose for 2 h, followed by immunoblot analysis (IB) as previously described [45], using anti-human PDGFR α (sc-338), PDGFR α -Y754 (sc-12911), PDGFR β (sc-339), PDGFR β -Y1021 (sc-12909) or neuropilin-1 (MAB38701) (R&D Systems). For quantification, densities of bands were determined using Gene Tools software (Syngene) and normalization to the corresponding loading control.

Phosphorylated PDGFR immunoassays

A cell-based human phospho-PDGFR β (Y751) ELISA kit (R&D Systems), was used to measure phosphorylated PDGFR β (Y751) and modified to measure phosphorylated PDGFR α (Y742) utilizing anti-phospho-PDGFR α (Y742) (AF2114) (R&D Systems). MSCs (10,000 cells/well) in serum-free medium were seeded onto 0.1% gelatin, stimulated with fresh

serum-free medium containing a specific growth factor, then immediately analysed according to the manufacturer's protocol. The phospho-PDGFR fluorescence at 600 nm in each well was normalized to the total-PDGFR fluorescence at 450 nm, and average triplicate readings determined.

Matrigel network formation assay

Round glass coverslips were coated with a thin-layer of growth factor reduced Matrigel (BD Biosciences), allowed to set, then seeded with MSCs (2×10^4) in 0.5% serum growth medium and incubated at 37°C. For quantitation of network formation, the average number of branch points/field after 24 h was determined. Each assay was performed in duplicate, with the number of branch points/field counted from at least six random fields per well.

CAM *in vivo* angiogenesis assay

Briefly, fertilized White Leghorn chicken eggs were incubated at 38°C for 5 days. Under aseptic conditions in a laminar flow cabinet, a small window at the top of the shell was carefully excised and the CAM blood vessels exposed. MSCs (2×10^4) were seeded onto a Matrigel coated coverslip and incubated for 45 min at 37°C to allow adherence. Coverslips were implanted MSCs face down onto a highly vascularized area of CAM, the shell opening sealed and the MSCs incubated *in ova* at 38°C for 24 h. Afterwards, coverslips were carefully removed from the CAM, washed in PBS, then processed for immunofluorescence microscopy.

Statistical analysis

In all quantitation experiments, results are expressed as the mean \pm standard deviation (SD).

Statistical differences between sets of data were determined by using a paired Student's *t* test on SigmaPlot 8.0 software, with $p < 0.05$ considered significant.

Accepted Manuscript

THIS IS NOT THE VERSION OF RECORD - see doi:10.1042/BJ20091512

RESULTS

PDGF ligands stimulated NRP-1 association with PDGFRs

We previously showed that multipotential MSCs which express PDGFRs α and β but no VEGFRs on their cell surface, also expressed NRP-1 [2, 4]. Using flow cytometry, we confirmed that MSCs express NRP-1 on their cell surface, but no VEGFR-2 (Fig. 1A).

Co-immunoprecipitation experiments were conducted to examine whether NRP-1 associates with PDGFR α and/or PDGFR β (Fig. 1B). NRP-1 co-immunoprecipitated with PDGFR α , and *vice versa*, predominantly in the presence of its ligands PDGF-AA, PDGF-BB or VEGF-A₁₆₅ (Fig. 1B (i,iii)). PDGFR β and NRP-1 co-immunoprecipitated in the presence of PDGF-BB or VEGF-A₁₆₅ (Fig. 1B (ii,iv)). These data demonstrate ligand regulation of the association of PDGFRs α and β with NRP-1.

To estimate the percentage of PDGFRs in a particular cell lysate which interact with NRP-1, co-immunoprecipitation analysis of total PDGFRs (Fig. 1C (i-ii)) and phosphorylated PDGFRs (Fig. 1C (iii-iv)), was evaluated. Using un-stimulated control MSCs, co-immunoprecipitation analysis demonstrated $\sim 5.0 \pm 0.7\%$ total PDGFR α or PDGFR β associated with NRP-1 (Fig. 1C (i-ii)), but MSC exposure to PDGF-AA resulted in $67 \pm 8\%$ total PDGFR α being associated with NRP-1, while exposure to PDGF-BB induced $36 \pm 7\%$ total PDGFR β to associate with NRP-1 (Fig. 1C (i-ii)) (Fig. 1D (i)). Similarly, co-immunoprecipitation analysis of PDGFR α phosphorylated at Y754 or PDGFR β at Y1021 (Fig. 1C (iii-iv)), demonstrated un-stimulated MSCs displayed $\sim 5.0 \pm 0.7\%$ phosphorylated PDGFRs associated with NRP-1, while exposure to PDGF-AA or PDGF-BB induced $63 \pm 6\%$ PDGFR α phosphorylated at Y754 and $31 \pm 6\%$ PDGFR β at Y1021 respectively, to associate with NRP-1 (Fig. 1C (iii-iv)) (Fig. 1D (ii)). These results are based on the proportion of receptor association within the immunoprecipitates. The values are likely to be indicative of total amounts of associated receptors, although the immunoprecipitation of each

receptor from a cell lysate may not be 100% efficient. Because the estimated proportions of total and phosphorylated PDGFRs which co-immunoprecipitated with NRP-1 in a particular cell lysate are comparable (see Figs 1D (i) and (ii)), the data suggest that virtually all the PDGFRs which associate with NRP-1 are phosphorylated.

NRP-1 co-localized with phosphorylated PDGFRs

To further demonstrate that PDGF ligand stimulation induces NRP-1 to associate with PDGFRs, we examined the cellular distribution of NRP-1 and phosphorylated PDGFRs by immunofluorescence microscopy.

Analysis of un-stimulated control MSCs demonstrated that PDGFR α -Y754 and PDGFR β -Y1021 immunoreactivity predominantly localized around perinuclear regions, but was also detected at low levels peripherally, while NRP-1 immunoreactivity had a wider cellular distribution which in some cases extended towards the cell surface (Fig. 2A,C). In contrast, MSCs exposed to PDGF-AA or PDGF-BB showed widespread cellular PDGFR α -Y754 (Fig. 2B), or PDGFR β -Y1021 (Fig. 2D) immunoreactivity respectively. Co-localization analysis of un-stimulated MSCs demonstrated minimal co-localization between NRP-1 and PDGFR α -Y754 and PDGFR β -Y1021, however, MSCs exposed to PDGF-AA or PDGF-BB resulted in a significant increase ($P < 0.001$, compared with un-stimulated control) in co-localization between NRP-1 and PDGFR α -Y754 or PDGFR β -Y1021 respectively (Fig. 2E), with PDGFR α -Y754 consistently producing the highest level of co-localization.

We also examined the cellular distribution of NRP-1 and total PDGFRs, using pan-PDGFR antibodies. In both un-stimulated control and ligand stimulated MSCs, while total PDGFR α immunoreactivity predominantly localized to perinuclear regions, total PDGFR β and NRP-1 immunoreactivity had a wider cellular distribution (Fig. S1A-D). Co-localization analysis demonstrated a low level of co-localization between NRP-1 and total PDGFRs in un-

stimulated MSCs, but a significant increase ($P < 0.001$, compared with un-stimulated control) on exposure to PDGF ligands (Fig. S1E), similar to the co-localization determined between NRP-1 and phosphorylated PDGFRs (Fig. 2E), but at a relatively lower level.

To compare the distribution of ligand stimulated NRP-1/PDGFR in MSCs with ligand induced NRP-1/VEGFR2 co-localization in endothelial cells (HUVECs), we examined VEGF-A₁₆₅ induced NRP-1/PDGFR α -Y754 and NRP-1/PDGFR β -Y1021 co-localization within MSCs, with VEGF-A₁₆₅ induced NRP-1/VEGFR2-Y1175 co-localization within HUVECs. While HUVECs generally displayed a wider NRP-1 distribution than MSCs, un-stimulated HUVECs and MSCs both demonstrated minimal NRP-1/VEGFR2 and NRP-1/PDGFR co-localization respectively (Fig. 3A,C,E). In contrast, VEGF-A₁₆₅ stimulation significantly increased ($P < 0.001$, compared with un-stimulated control) the co-localization of NRP-1 with VEGFR2-Y1175 in HUVECs (Fig. 3B), as well as NRP-1 with PDGFR α -Y754 (Fig. 3D) and PDGFR β -Y1021 (Fig. 3F) in MSCs.

Thus in MSCs, PDGF and VEGF-A₁₆₅ ligands induce co-localization of NRP-1 with phosphorylated PDGFRs, similar to VEGF-A₁₆₅ induced NRP-1 co-localization with phosphorylated VEGFR2 in HUVECs.

NRP-1 regulated ligand-induced PDGFR phosphorylation

Having established that NRP-1 can associate and co-localize with phosphorylated PDGFR α and PDGFR β , we investigated whether NRP-1 regulates PDGFR signaling. Following NRP-1 knockdown using two different siRNAs, NRP-1 protein expression was virtually ablated (Fig. 4A), while RT-PCR analysis of their targeting specificity demonstrated they did not affect PDGFR transcripts (Fig. 4B). We therefore utilized NRP-1 knockdown during this study, first examining PDGFR α phosphorylation levels in serum-free conditions, using an ELISA for PDGFR α (Y742). NRP-1 knockdown had little impact on basal levels of un-stimulated

PDGFR α phosphorylation (Fig. 4C). However, exposure to PDGF-AA strongly stimulated PDGFR α phosphorylation, with NRP-1 knockdown dramatically reducing this phosphorylation to near-basal levels (Fig. 4C). While PDGF-CC and VEGF-A₁₆₅ stimulated lower levels of PDGFR α phosphorylation, NRP-1 knockdown also reduced their phosphorylation to near-basal levels (Fig. 4C). Thus, NRP-1 markedly regulates PDGFR α signaling when stimulated by these growth factors. However, NRP-1 knockdown did not inhibit PDGF-AB stimulated PDGFR α phosphorylation. The differential effects of NRP-1 knockdown on PDGF-CC and PDGF-AB induced PDGFR α phosphorylation reflect these growth factor binding specificities; PDGF-CC can bind the PDGFR $\alpha\alpha$ homodimer and PDGFR $\alpha\beta$ heterodimer [35, 46], whereas PDGF-AB mainly binds PDGFR $\alpha\beta$ [36]. These results thus imply ligand-induced NRP-1 dependent PDGFR α homodimer signaling.

We also investigated whether NRP-1 regulates PDGFR β signaling in serum-free conditions using an ELISA for PDGFR β (Y751). Control scrambled and target NRP-1 siRNA knockdowns resulted in comparable basal levels of un-stimulated PDGFR β phosphorylation (Fig. 4D). While exposure to PDGF-BB strongly stimulated PDGFR β phosphorylation, NRP-1 knockdown only partially reduced this phosphorylation (Fig. 4D). However, while VEGF-A₁₆₅ stimulated lower levels of PDGFR β phosphorylation, NRP-1 knockdown effectively inhibited this phosphorylation. Thus NRP-1 also regulates ligand-induced PDGFR β phosphorylation. Since NRP-1 knockdown only decreased PDGF-BB induced PDGFR β phosphorylation by $\sim 44 \pm 5 \%$, we examined whether NRP-1 knockdown primarily affects PDGF-BB-induced PDGFR $\alpha\beta$ phosphorylation, using PDGF-AB and PDGF-CC which bind the PDGFR $\alpha\beta$ heterodimer but not a PDGFR $\beta\beta$ homodimer [35-36, 46]. While both of these ligands induced PDGFR β phosphorylation, indicating heterodimer stimulation, NRP-1

knockdown had no inhibitory effect in either case (Fig. 4D). These results thus imply that NRP-1 influences ligand-induced PDGFR β homodimer signaling.

NRP-1 regulated PDGFR-induced MSC migration and proliferation

Having established that NRP-1 plays a prominent role in regulating ligand-induced PDGFR signaling, the functional importance of this receptor crosstalk was investigated. We previously demonstrated that VEGF-A or PDGF induced PDGFR signaling stimulates migration of MSCs [2]. Here we examined in serum-free conditions, whether NRP-1 regulates PDGFR mediated MSC migration. In the absence of ligand, control scrambled and target NRP-1 siRNA knockdowns resulted in comparable basal levels of un-stimulated MSC migration (Fig. 5A,B), similar to NRP-1 effects on PDGFR phosphorylation (Fig. 4C,D). Exposure to PDGF-AA (PDGFR α homodimer mediated) increased MSC migration, but was inhibited to virtually basal levels by NRP-1 knockdown (Fig. 5A,B). Likewise, NRP-1 knockdown also decreased PDGF-BB and VEGF-A₁₆₅ induced MSC migration, by $\sim 38 \pm 6$ % and $\sim 56 \pm 8$ % respectively (Fig. 5A,B). Control scrambled and NRP-1 knockdowns in the presence or absence of a VEGFR2 tyrosine kinase inhibitor, produced a similar level of VEGF-A₁₆₅ induced MSC migration (Fig. 5B), indicating that a VEGFR2/NRP-1 complex was not contributing to VEGF-A₁₆₅ stimulated MSC migration. NRP-1 had minimal effect on PDGF-CC or PDGF-AB induced MSC migration, confirming that these ligands probably stimulate migration through PDGFR $\alpha\beta$, but independently of NRP-1 (data not shown).

We also investigated the effects of NRP-1 knockdown on serum stimulated MSC proliferation, in the absence or presence of supplementary PDGFR ligands. In serum growth medium alone, scrambled knockdown control MSCs proliferated up to 5 days, which was increased by supplementary PDGF-AA (Fig. 5C) or PDGF-BB (Fig. 5D). In comparison, at each time point NRP-1 knockdown significantly inhibited serum stimulated MSC

proliferation (Fig. 5C,D). Moreover, NRP-1 knockdown decreased serum and PDGF-ligand supplemented proliferation to comparable levels (Fig. 5C,D), indicating that NRP-1 knockdown was inhibiting PDGF ligand stimulated MSC proliferation. Similar results were obtained following NRP-1 knockdown of serum stimulated MSC proliferation, in the absence or presence of supplementary VEGF-A₁₆₅ (data not shown).

These results highlight the crucial contribution of NRP-1 to ligand-induced PDGFR-mediated MSC migration and proliferation.

NRP-1 regulated the assembly of MSC networks in Matrigel

MSCs are critical contributors to neovascularization [47], and NRP-1 and PDGFRs play essential roles in this process [11, 41]. Having established that NRP-1 plays a crucial role in regulating PDGFR mediated MSC phosphorylation, migration and proliferation, we went on to examine the function of NRP-1 in regulating the assembly of MSC network formation in a Matrigel culture model over 24 hours.

We first evaluated the distribution of NRP-1 and phosphorylated PDGFRs during MSC network assembly, by determining the immunolocalization of NRP-1 and PDGFR α -Y754 or PDGFR β -Y1021. During the initial stages of network assembly, MSCs exhibited intense widespread NRP-1 immunoreactivity (Fig. 6). After 2 hours seeding onto Matrigel, high levels of PDGFR α -Y754 immunoreactivity were predominantly localized around the cell surface, where it conspicuously co-localized with NRP-1 (Fig. 6A). In comparison, PDGFR β -Y1021 was distributed throughout the cell, including the cell surface, but co-localization with NRP-1 was at a lower level (Fig. 6B). After 6 hours, PDGFR α -Y754 and NRP-1 co-localization had a wider cellular distribution (Fig. 6C), while co-localization of PDGFR β -Y1021 with NRP-1 became more prominent, especially at the cell surface (Fig. 6D). By 24 hours, MSCs had assembled to form abundant capillary-like network structures, which

displayed high levels of co-localized NRP-1 with PDGFR α -Y754 and PDGFR β -Y1021 (Fig. 6E,F). To further substantiate these data, NRP-1 was also shown to co-localize with PDGFR α -Y720 and PDGFR β -Y751 in MSC networks (Fig. S2A,B).

We confirmed that VEGFR2-Y1175 was not expressed in MSC networks (Fig. S3A). However, HUVECs in Matrigel readily formed capillary-like network structures, as expected, which not only displayed prominent co-localization of NRP-1 with VEGFR2-Y1175 (Fig. S3B), but also with PDGFR α -Y754 and PDGFR β -Y1021 (Fig. S3C,D), suggesting that PDGFRs may also influence NRP-1 function in endothelial cells.

Having demonstrated that NRP-1 regulates PDGFR signaling and both receptors are abundantly co-localized within MSC network structures, we went on to examine MSC network assembly following NRP-1 knockdown (Fig. 7). Control scrambled knockdown MSCs formed widespread capillary-like network structures within 24 hours, containing pronounced NRP-1, PDGFR α -Y754 and PDGFR β -Y1021 immunoreactivity and co-localization (Fig. 7A,C,E), comparable to un-transfected MSCs (see Figs. 6E,F). However after 24 hours, NRP-1 knockdown MSCs produced distinctly disorganized structures (Fig. 7B,D,F), containing significantly fewer branch points compared to control MSCs (Fig. 7G). As expected, there was a dramatic reduction in NRP-1 immunoreactivity, confirming the efficiency of the knockdown, concurrent with a distinct decrease in both PDGFR α -Y754 and PDGFR β -Y1021 immunoreactivity (Fig. 7B,D).

These results indicate that NRP-1 regulation of PDGFR signaling plays a crucial role in directing MSC network assembly.

NRP-1 regulated the assembly of MSC networks in a chorioallantoic membrane model

To further demonstrate the importance of NRP-1 during MSC network formation, we examined the effects of NRP-1 knockdown utilizing an *in vivo* angiogenesis model system;

the chorioallantoic membrane (CAM) of the developing chicken embryo [48]. Control scrambled or NRP-1 knockdown MSCs were seeded onto Matrigel, then implanted in contact with a highly vascularized area of CAM for 24 hours. As a control, identically prepared MSCs were also cultured *in vitro*. Following intimate association with the underlying CAM blood vessel microenvironment for 24 hours, control MSCs formed widespread capillary-like network structures, containing abundant NRP-1, PDGFR α -Y754 and PDGFR β -Y1021 immunoreactivity (Fig. 8A,C,E,F). Both PDGFR α -Y754 and PDGFR β -Y1021 displayed a high level of co-localization with NRP-1 in these *in vivo* assembled networks (Fig. 8E,F), similar to the control *in vitro* cultured MSCs (data not shown) as previously demonstrated (see Fig. 7A,C). In striking contrast however, after 24 hours CAM exposure, NRP-1 knockdown resulted in widespread clusters of MSCs maintaining a rounded cellular morphology, which only exhibited trace levels of NRP-1, PDGFR α -Y754 or PDGFR β -Y1021 immunoreactivity (Fig. 8B,D). In comparison, the control *in vitro* cultured NRP-1 knockdown MSCs produced highly disorganized network assemblies (data not shown) as previously demonstrated (see Fig. 7B,D).

Thus NRP-1 is critical for PDGFR signaling and the *in vivo* assembly of MSC network structures within the CAM vasculature microenvironment.

Accepted Manuscript

DISCUSSION

MSCs, which offer immense potential for cell-based tissue regeneration, have the capability to differentiate along vascular cell lineages [1-3]. Previously, we showed that multipotent human MSCs express NRP-1 and PDGFRs but not VEGFRs, and that PDGFs regulate MSC proliferation and migration, and smooth muscle-specific cytoskeleton [2, 4]. PDGFR α is an essential regulator of mesenchymal tissue formation in early embryonic development [38], and both PDGFRs contribute to vessel wall development and remodeling following injury [42]. The essential contribution of NRP-1 to vascular development and neovascularization is also well documented [11] and, whilst its mechanisms of action remain incompletely understood, it is thought to regulate cell surface receptor clustering and signaling in a ligand-dependent manner. Our discovery that NRP-1 regulates the phosphorylation and signaling responses of PDGFRs, especially PDGFR α , sheds important light on fundamental cellular mechanisms of tissue development and neovascularization.

NRP-1 co-immunoprecipitated and co-localized with phosphorylated PDGFRs, and this association was significantly increased in the presence of growth factor ligands, indicating that the PDGFR crosstalk with NRP-1 that we have identified may occur through a receptor-bridging mechanism. Indeed, *in vitro* binding studies indicate that PDGFR α and NRP-1 do not interact directly, but PDGF ligands, PDGF-AA, PDGF-BB and VEGF-A₁₆₅ all bind NRP-1 (Fig. S4). PDGF-AA mediated PDGFR α responses were particularly dependent upon NRP-1, implying that NRP-1 may be indispensable for PDGFR α function in tissue development and remodeling. PDGFR β dependence on NRP-1 was also significant, so NRP-1 must regulate PDGFR β -dependent smooth muscle cell migration, proliferation, and differentiation during vessel wall maturation and repair.

While NRP-1 is a transmembrane protein, immunofluorescence analysis demonstrated that the majority of NRP-1 in permeabilized MSCs and HUVECs was localized intracellular. Exposure to VEGF-A₁₆₅ has been shown to promote neuropilin-1 on the surface of HUVECs to internalize, with immunofluorescence analysis of the permeabilized HUVECs demonstrating neuropilin-1 predominantly localized around perinuclear regions [50]. Thus a similar mechanism resulting in rapid ligand-induced NRP-1 internalization may occur in MSCs.

MSCs readily formed extensive networks in matrigel and CAM assays, highlighting their potential to contribute to blood vessel formation. Co-localization of NRP-1 with phosphorylated PDGFRs occurred prominently in these networks, and the essential role for NRP-1/PDGFR crosstalk in network formation was confirmed by knockdown of NRP-1 which caused dramatically reduced PDGFR phosphorylation and grossly disrupted network formation. Prominent pericellular co-localization of NRP-1 with PDGFR α during early network formation suggests that this relationship is particularly important in initiating cellular changes leading to network formation. In MSCs, VEGF-A also induced NRP-1/PDGFR co-localization, similar to VEGF-A induced NRP-1 co-localization with VEGFR2 in HUVECs. Since in HUVECs, NRP-1 co-localized with both VEGFR2 and PDGFRs in response to VEGF-A, NRP-1/PDGFR crosstalk is likely to contribute to endothelial functions mediated by VEGF-A. Our MSCs do not express VEGFRs so their response to PDGFs and VEGF-A ligands is channelled through PDGFRs, but in endothelial and other cells expressing both VEGFRs and PDGFRs, the relative abundance of each receptor, local ligand concentrations and receptor affinities may combine to modify NRP-1-dependent receptor signals.

The essential contribution of PDGFR α to the formation of embryonic mesoderm and mesenchymal tissues is well documented [34], and we have demonstrated a high PDGFR α : β ratio in our MSCs [4]. PDGFR α null mice die around E10 due to vascular and other defects [40], whilst conditional null mice highlight that both PDGFRs are essential for early yolk sac vascular development [41]. The NRP-1 knockout mouse is also embryonic lethal, with major yolk sac and embryonic vascular defects, dying between E10 to E12.5 [49]. Thus, the functional crosstalk between NRP-1 and both PDGFRs, especially PDGFR α , that we have identified, suggests a fundamental developmental relationship between these receptors.

In summary, we have shown ligand-dependent crosstalk between NRP-1 and phosphorylated PDGFRs that controls receptor signaling, migration, network formation and proliferation of MSCs. We have thus identified NRP-1 as an essential co-receptor for PDGFR signaling, which may critically contribute to the formation of blood vessels and other mesenchymal tissues. This mechanism may be exploited in the application of MSCs in tissue regeneration.

ACKNOWLEDGEMENTS

We thank Ms Jemima Whyte (University of Manchester) for her contribution towards developing the CAM assay, and Ms Maybo Chiu for recombinant VEGF-A used in the binding assays.

Accepted Manuscript

THIS IS NOT THE VERSION OF RECORD - see doi:10.1042/BJ20091512

FUNDING

This work was funded by the Medical Research Council (UK) (G0700712). CMK holds a Royal Society Wolfson Research Merit award.

Accepted Manuscript

THIS IS NOT THE VERSION OF RECORD - see doi:10.1042/BJ20091512

REFERENCES

1. Oswald, J., Boxberger, S., Jorgensen, B., Feldmann, S., Ehninger, G., Bornhauser, M., and Werner, C. (2004) Mesenchymal stem cells can differentiate into endothelial cells in vitro. *Stem Cells* **22**, 377-384
2. Ball, S.G., Shuttleworth, C.A. and Kielty, C.M. (2007a). Vascular endothelial growth factor can signal through platelet-derived growth factor receptors. *J. Cell Biol.* **177**, 489-500
3. Chen, M.Y., Lie, P.C., Li, Z.L. and Wei, X. (2009). Endothelial differentiation of Wharton's jelly-derived mesenchymal stem cells in comparison with bone marrow-derived mesenchymal stem cells. *Exp. Hematol.* **37**, 629-640
4. Ball, S.G., Shuttleworth, C.A. and Kielty, C.M. (2007b). Platelet-derived growth factor receptor-alpha is a key determinant of smooth muscle alpha-actin in bone marrow-derived mesenchymal stem cells. *Int. J. Biochem. Cell Biol.* **39**, 379-391.
5. Chen, H., Chedotal, A., He, Z., Goodman, C.S. and Tessier-Lavigne, M. (1997). Neuropilin-2, a novel member of the neuropilin family, is a high affinity receptor for the semaphorins Sema E and Sema IV but not Sema III. *Neuron* **19**, 547-559
6. Kolodkin, A.L., Levengood, D.V., Rowe, E.G., Tai, Y.T., Giger, R.J. and Ginty, D.D. (1997). Neuropilin is a semaphorin III receptor. *Cell* **90**, 753-62

7. Soker, S., Takashima, S., Miao, H.Q., Neufeld, G. and Klagsbrun, M. (1998). Neuropilin-1 is expressed by endothelial and tumor cells as an isoform-specific receptor for vascular endothelial growth factor. *Cell* **92**, 735-45
8. Takahashi, T., Nakamura, F., Jin, Z., Kalb, R.G. and Strittmatter, S.M. (1998). Semaphorins A and E act as antagonists of neuropilin-1 and agonists of neuropilin-2 receptors. *Nat. Neurosci.* **1**, 487-493
9. Serini, G., Valdembri, D., Zanivan, S., Morterra, G., Burkhardt, C., Caccavari, F., Zammataro, L., Primo, L., Tamagnone, L., Logan, M., Tessier-Lavigne, M., Taniguchi, M., Puschel, A.W. and Bussolino, F. (2003). Class 3 semaphorins control vascular morphogenesis by inhibiting integrin function. *Nature* **424**, 391-397
10. Gitler, A.D., Lu, M.M. and Epstein, J.A. (2004). PlexinD1 and semaphorin signaling are required in endothelial cells for cardiovascular development. *Dev. Cell* **7**, 107-116
11. Pellet-Many, C., Frankel, P., Jia, H. and Zachary, I. (2008). Neuropilins: structure, function and role in disease. *Biochem. J.* **411**, 211-216
12. Kitsukawa, T., Shimono, A., Kawakami, A., Kondoh, H. and Fujisawa, H. (1995). Overexpression of a membrane protein, neuropilin, in chimeric mice causes anomalies in the cardiovascular system, nervous system and limbs. *Development* **121**, 4309-18

13. Kawasaki, T., Kitsukawa, T., Bekku, Y., Matsuda, Y., Sanbo, M., Yagi, T. and Fujisawa, H. (1999). A requirement for neuropilin-1 in embryonic vessel formation. *Development* **126**, 4895-902
14. Lee, P., Goishi, K., Davidson, A.J., Mannix, R., Zon, L. and Klagsbrun, M. (2002). Neuropilin-1 is required for vascular development and is a mediator of VEGF-dependent angiogenesis in zebrafish. *Proc. Natl. Acad. Sci. U S A.* **99**, 10470-10475
15. Cai, H. and Reed, R.R. (1999). Cloning and characterization of neuropilin-1-interacting protein: a PSD-95/Dlg/ZO-1 domain-containing protein that interacts with the cytoplasmic domain of neuropilin-1. *J. Neurosci.* **19**, 6519-6527
16. Wang, L., Mukhopadhyay, D. and Xu, X. (2006). C terminus of RGS-GAIP-interacting protein conveys neuropilin-1-mediated signaling during angiogenesis. *FASEB J.* **20**, 1513-1515
17. Bielenberg, D.R., Pettaway, C.A., Takashima, S. and Klagsbrun, M. (2006). Neuropilins in neoplasms: expression, regulation, and function. *Exp. Cell Res.* **312**, 584-593
18. Guttman-Raviv, N., Kessler, O., Shraga-Heled, N., Lange, T., Herzog, Y. and Neufeld, G. (2006). The neuropilins and their role in tumorigenesis and tumor progression. *Cancer Lett.* **231**, 1-11

19. Geretti, E., Shimizu, A. and Klagsbrun, M. (2008). Neuropilin structure governs VEGF and semaphorin binding and regulates angiogenesis. *Angiogenesis* **11**, 31-39
20. Pan, Q., Chathery, Y., Wu, Y., Rathore, N., Tong, R.K., Peale, F., Bagri, A., Tessier-Lavigne, M., Koch, A.W. and Watts, R.J. (2007). Neuropilin-1 binds to VEGF121 and regulates endothelial cell migration and sprouting. *J. Biol. Chem.* **282**, 24049-24056
21. Salikhova, A., Wang, L., Lanahan, A.A., Liu, M., Simons, M., Leenders, W.P., Mukhopadhyay, D. and Horowitz, A. (2008). Vascular endothelial growth factor and semaphorin induce neuropilin-1 endocytosis via separate pathways. *Circ. Res.* **103**, e71-79
22. Whitaker, G.B., Limberg, B.J. and Rosenbaum, J.S. (2001). Vascular endothelial growth factor receptor-2 and neuropilin-1 form a receptor complex that is responsible for the differential signaling potency of VEGF(165) and VEGF(121). *J. Biol. Chem.* **276**, 25520-25531
23. Neufeld, G., Kessler, O., and Herzog, Y. (2002) The interaction of Neuropilin-1 and Neuropilin-2 with tyrosine-kinase receptors for VEGF. *Adv. Exp. Med. Biol.* **515**, 81-90
24. Soker, S., Miao, H.Q., Nomi, M., Takashima, S. and Klagsbrun, M. (2002). VEGF165 mediates formation of complexes containing VEGFR-2 and neuropilin-1 that enhance VEGF165-receptor binding. *J. Cell Biochem.* **85**, 357-368

25. Shraga-Heled, N., Kessler, O., Prahst, C., Kroll, J., Augustin, H. and Neufeld, G. (2007). Neuropilin-1 and neuropilin-2 enhance VEGF121 stimulated signal transduction by the VEGFR-2 receptor. *FASEB J.* **21**, 915-926
26. Kawamura, H., Li, X., Goishi, K., van Meeteren, L.A., Jakobsson, L., Cebe-Suarez, S., Shimizu, A., Edholm, D., Ballmer-Hofer, K., Kjellen, L., Klagsbrun, M. and Claesson-Welsh, L. (2008). Neuropilin-1 in regulation of VEGF-induced activation of p38MAPK and endothelial cell organization. *Blood* **112**, 3638-3649
27. Prahst, C., Heroult, M., Lanahan, A.A., Uziel, N., Kessler, O., Shraga-Heled, N., Simons, M., Neufeld, G. and Augustin, H.G. (2008). Neuropilin-1-VEGFR-2 complexing requires the PDZ-binding domain of neuropilin-1. *J. Biol. Chem.* **283**, 25110-25114
28. Bachelder, R.E., Crago, A., Chung, J., Wendt, M.A., Shaw, L.M., Robinson, G. and Mercurio, A.M. (2001). Vascular endothelial growth factor is an autocrine survival factor for neuropilin-expressing breast carcinoma cells. *Cancer Res.* **61**, 5736-5740
29. Bachelder, R.E., Wendt, M.A. and Mercurio, A.M. (2002). Vascular endothelial growth factor promotes breast carcinoma invasion in an autocrine manner by regulating the chemokine receptor CXCR4. *Cancer Res.* **62**, 7203-7206
30. West, D.C., Rees, C.G., Duchesne, L., Patey, S.J., Terry, C.J., Turnbull, J.E., Delehedde, M., Heegaard, C.W., Allain, F., Vanpouille, C., Ron, D. and Fernig, D.G. (2005). Interactions of multiple heparin binding growth factors with neuropilin-1 and

potentiation of the activity of fibroblast growth factor-2. *J. Biol. Chem.* **280**, 13457-13464

31. Sulpice, E., Plouet, J., Berge, M., Allanic, D., Tobelem, G. and Merkulova-Rainon, T. (2008). Neuropilin-1 and neuropilin-2 act as coreceptors, potentiating proangiogenic activity. *Blood* **111**, 2036-2045
32. Banerjee, S., Sengupta, K., Dhar, K., Mehta, S., D'Amore, P.A., Dhar, G. and Banerjee, S.K. (2006). Breast cancer cells secreted platelet-derived growth factor-induced motility of vascular smooth muscle cells is mediated through neuropilin-1. *Mol. Carcinog.* **45**, 871-880
33. Holmes, D.I. and Zachary, I. (2005). The vascular endothelial growth factor (VEGF) family: angiogenic factors in health and disease. *Genome Biol.* **6**, 209-219
34. Andrae, J., Gallini, R. and Betsholtz, C. (2008). Role of platelet-derived growth factors in physiology and medicine. *Genes Dev.* **22**, 1276-1312
35. Fredriksson, L., Li, H. and Eriksson, U. (2004). The PDGF family: four gene products form five dimeric isoforms. *Cytokine Growth Factor Rev.* **15**, 197-204
36. Zhang, J., Cao, R., Zhang, Y., Jia, T., Cao, Y. and Wahlberg, E. (2009). Differential roles of PDGFR-alpha and PDGFR-beta in angiogenesis and vessel stability. *FASEB J.* **23**, 153-163

37. Palmieri, S.L., Payne, J., Stiles, C.D., Biggers, J.D. and Mercola, M. (1992).
Expression of mouse PDGF-A and PDGF alpha-receptor genes during pre- and post-implantation development: evidence for a developmental shift from an autocrine to a paracrine mode of action. *Mech. Dev.* **39**, 181-191
38. Soriano, P. (1997). The PDGF alpha receptor is required for neural crest cell development and for normal patterning of the somites. *Development* **124**, 2691-2700
39. Darabi, R., Gehlbach, K., Bachoo, R.M., Kamath, S., Osawa, M., Kamm, K.E. and Perlingeiro, R.C. (2008). Functional skeletal muscle regeneration from differentiating embryonic stem cells. *Nature Med.* **14**, 134-143
40. Bostrom, H., Willetts, K., Pekny, M., Leveen, P., Lindahl, P., Hedstrand, H., Pekna, M., Hellstrom, M., Gebre-Medhin, S., Schalling, M., Nilsson, M., Kurland, S., Tornell, J., Heath, J.K. and Betsholtz, C. (1996). PDGF-A signaling is a critical event in lung alveolar myofibroblast development and alveogenesis. *Cell* **85**, 863-873
41. French, W.J., Creemers, E.E. and Tallquist, M.D. (2008). Platelet-derived growth factor receptors direct vascular development independent of vascular smooth muscle cell function. *Mol. Cell Biol.* **28**, 5646-5657
42. Raines, E.W. (2004). PDGF and cardiovascular disease. *Cytokine Growth Factor Rev.* **15**, 237-254

43. Cimato, T., Beers, J., Ding, S., Ma, M., McCoy, J.P., Boehm, M. and Nabel, E.G. (2009). Neuropilin-1 identifies endothelial precursors in human and murine embryonic stem cells before CD34 expression. *Circulation* **119**, 2170-2178
44. Zacchigna, S., Pattarini, L., Zentilin, L., Moimas, S., Carrer, A., Sinigaglia, M., Arsic, N., Tafuro, S., Sinagra, G. and Giacca, M. J. (2008). Bone marrow cells recruited through the neuropilin-1 receptor promote arterial formation at the sites of adult neoangiogenesis in mice. *J. Clin. Invest.* **118**, 2062-2075
45. Ball, S.G., Shuttleworth, C.A. and Kielty, C.M. (2004). Direct cell contact influences bone marrow mesenchymal stem cell fate. *Int. J. Biochem. Cell Biol.* **36**, 714-727
46. Gilbertson, D.G., Duff, M.E., West, J.W., Kelly, J.D., Sheppard, P.O., Hofstrand, P.D., Gao, Z., Shoemaker, K., Bukowski, T.R., Moore, M., Feldhaus, A.L., Humes, J.M., Palmer, T.E. and Hart, C.E. (2001). Platelet-derived growth factor C (PDGF-C), a novel growth factor that binds to PDGF alpha and beta receptor. *J. Biol. Chem.* **276**, 27406-27414
47. Silva, G.V., Litovsky, S., Assad, J.A., Sousa, A.L., Martin, B.J., Vela, D., Coulter, S.C., Lin, J., Ober, J., Vaughn, W.K., Branco, R.V., Oliveira, E.M., He, R., Geng, Y.J., Willerson, J.T. and Perin, E.C. (2005). Mesenchymal stem cells differentiate into an endothelial phenotype, enhance vascular density, and improve heart function in a canine chronic ischemia model. *Circulation* **111**, 150-156

48. Ribatti, D., Vacca, A., Roncali, L. and Dammacco, F. (1996). The chick embryo chorioallantoic membrane as a model for in vivo research on angiogenesis. In. *J. Dev. Biol.* **40**, 1189-1197
49. Takashima, S., Kitakaze, M., Asakura, M., Asanuma, H., Sanada, S., Tashiro, F., Niwa, H., Miyazaki Ji, J., Hirota, S., Kitamura, Y., Kitsukawa, T., Fujisawa, H., Klagsbrun, M. and Hori, M. (2002). Targeting of both mouse neuropilin-1 and neuropilin-2 genes severely impairs developmental yolk sac and embryonic angiogenesis. *Proc. Natl. Acad. Sci. USA.* **99**, 3657-3662
50. Narazaki, M. and Tosato, G. (2006). Ligand-induced internalization selects use of common receptor neuropilin-1 by VEGF₁₆₅ and semaphorin3A. *Blood* **107**, 3892-3901
51. Goretzki, L., Burg, M.A., Grako, K.A. and Stallcup, W.B. (1999). High-affinity binding of basic fibroblast growth factor and platelet-derived growth factor-AA to the core protein of the NG2 proteoglycan. *J. Biol. Chem.* **274**, 16831-16837

FIGURE LEGENDS

Figure 1. NRP-1 associated with phosphorylated PDGFRs

The association of NRP-1 with PDGFRs was evaluated. **(A)** Flow cytometry analysis of cell surface **(i)** IgG₁ used as a control, **(ii)** NRP-1 and **(iii)** VEGFR2. A representative example of three independent experiments is shown. **(B)** The association of NRP-1 with PDGFRs was examined by immunoprecipitation (IP) followed by immunoblot (IB) analysis. MSCs grown on gelatin and cultured for 24 h in serum-free conditions were un-stimulated (Con) or stimulated with either 20 ng/ml PDGF-AA, PDGF-BB or VEGF-A₁₆₅ for 10 min at 37°C, then NRP-1 association with PDGFRs determined by IP analysis of cell lysates. IP analysis using **(i-ii)** anti-NRP-1 **(iii)** anti-PDGFR α or **(iv)** anti-PDGFR β , with anti-IgG₁ as a control, then NRP-1 association with PDGFRs detected by IB analysis using **(i)** anti-PDGFR α , **(ii)** anti-PDGFR β or **(iii-iv)** anti-NRP-1, followed by IB analysis using anti-PDGFRs or NRP-1 as loading controls. A representative of three independent experiments is shown. **(C)** The percentage of **(i-ii)** total PDGFRs and **(iii-iv)** phosphorylated PDGFRs interacting with NRP-1 in a particular cell lysate was estimated by IP and IB analysis. Cell lysates were isolated from MSCs which were either un-stimulated (Con) (lysates 1 and 3), or exposed to 20 ng/ml PDGF-AA (lysate 2), or PDGF-BB (lysate 4) for 10 min at 37°C. Each cell lysate was then split into four separate 100 μ g aliquots (i-iv) for IP analysis, using either anti-NRP-1, anti-PDGFR α (R α) or anti-PDGFR β (R β), then IB analysis using (i-ii) anti-PDGFR α or anti-PDGFR β and (iii-iv) using anti-PDGFR α -Y754 or anti-PDGFR β -Y1021. As a loading control blots were re-probed using the corresponding IP antibody. The percentage of total PDGFR α or PDGFR β interacting with NRP-1 was estimated by quantifying the IB analysis in (i) relative to the corresponding IB analysis in (ii), which was assumed to be 100%. Similarly, the percentage of phosphorylated PDGFR α -Y754 or PDGFR β -Y1021 interacting with NRP-1 was estimated by quantifying the IB analysis in (iii) relative to the corresponding IB analysis

in (iv), which was taken to be 100%. This approach gives the proportion of receptor association within the immunoprecipitates, but does not report the total amounts of receptors since the efficiency of each antibody in immunoprecipitating their receptor from a cell lysate may not be 100%. **(D)** Bar graph representing the co-immunoprecipitation data, showing the percentage of **(i)** total PDGFR α or PDGFR β and **(ii)** phosphorylated PDGFR α -Y754 or PDGFR β -Y1021, which interacted with NRP-1. Data shown is mean percentage values \pm SD determined from two independent experiments. ** $P < 0.001$, compared with un-stimulated control.

Figure 2. NRP-1 co-localized with phosphorylated PDGFRs

The cellular distribution of NRP-1 and phosphorylated PDGFRs was examined following ligand exposure. MSCs grown on 0.1% gelatin were cultured for 24 h in serum-free conditions, exposed to PDGF ligands, then co-localization of NRP-1 with either phosphorylated PDGFR α at site Y754, or PDGFR β at site Y1021, examined by immunofluorescence microscopy. **(A)** Control un-stimulated and **(B)** exposed to 20 ng/ml PDGF-AA for 10 min, showing PDGFR α -Y754 (green) and NRP-1 (red). **(C)** Control un-stimulated and **(D)** exposed to 20 ng/ml PDGF-BB for 10 min, showing PDGFR β -Y1021 (red) and NRP-1 (green). For each image, the corresponding red and green channels having similar threshold values and the same particle size range are shown, together with their co-localization represented by the image in yellow. The mean number of co-localized particles \pm SD derived from six different single cell images is denoted in yellow. Nuclei are counter-stained with DAPI (blue). Representative images of at least four independent experiments are shown. Scale bars = 20 μ m. **(E)** Bar graph showing ligand induced increase in co-localization between NRP-1 and PDGFR α -Y754 or PDGFR β -Y1021, as determined by immunofluorescence analysis. Data shown is mean number of co-localized particles \pm SD derived from six different single cell images. ** $P < 0.001$, compared with corresponding un-stimulated control.

Figure 3. Comparison of VEGF-A stimulated MSCs and HUVECs

The cellular distribution of NRP-1 was examined in MSCs and compared to HUVECs following VEGF-A₁₆₅ stimulation. MSCs grown on 0.1% gelatin were cultured for 24 h in serum-free conditions, then co-localization of NRP-1 with either PDGFR α at site Y754, or PDGFR β at site Y1021, examined by immunofluorescence microscopy. As a comparison, HUVECs grown on 0.1% gelatin were cultured for 4 h in serum-free conditions, then co-localization of NRP-1 with VEGFR2 at site Y1175 similarly determined. **(A)** Control un-stimulated HUVEC and **(B)** HUVEC exposed to VEGF-A₁₆₅ for 10 min, showing VEGFR2-Y1175 (red) and NRP-1 (green). **(C)** Control un-stimulated MSC and **(D)** MSC exposed to VEGF-A₁₆₅ for 10 min, showing PDGFR α -Y754 (green) and NRP-1 (red). **(E)** Control un-stimulated MSC and **(F)** MSC exposed to 20 ng/ml VEGF-A₁₆₅ for 10 min, showing PDGFR β -Y1021 (red) and NRP-1 (green). Below each image, the corresponding red and green channels which have similar threshold values and the same particle size range are shown, together with their co-localization represented by the image in yellow. The mean number of co-localized particles \pm SD derived from four different single cell images is denoted in yellow. ** $P < 0.001$, compared with corresponding un-stimulated control. Nuclei are counter-stained with DAPI (blue). Representative images of at least three independent experiments are shown. Scale bars = 20 μ m.

Figure 4. NRP-1 enhanced PDGFR phosphorylation

The effects of NRP-1 knockdown on PDGFR phosphorylation was determined. **(A)** Lysates from MSCs transfected with two different NRP-1 siRNAs, **(i)** (from Qiagen) **(ii)** (from Ambion), or scrambled (Scr) control, were analysed for NRP-1 protein expression by IB analysis using anti-NRP-1 antibody. Membranes were reprobbed with anti- β actin as a loading control. **(B)** The targeting specificity of each siRNA knockdown was evaluated by RT-PCR analysis. Following siRNA knockdown using Scr control or two different NRP-1 siRNAs **(i)** (from Qiagen), **(ii)** (from Ambion), transcript expression for PDGFR α , PDGFR β , NRP-1 and GAPDH as a control were determined. A representative of two independent experiments are shown. **(C,D)** Following siRNA knockdown with either Scr control or target NRP-1 siRNAs, MSCs in serum-free medium were exposed to either 50 ng/ml PDGF-AA, PDGF-BB, PDGF-AB, PDGF-CC or VEGF-A₁₆₅, or no growth factors (basal) for 10 minutes at 37°C, then specific PDGFR tyrosine phosphorylation determined by cell-based ELISAs **(C)** PDGFR α (Y742) or **(D)** PDGFR β (Y751). Tyrosine phosphorylation is represented by relative fluorescent units (RFU). Data shown are mean normalized RFU \pm SD determined from two independent experiments performed in triplicate, using two different NRP-1 siRNAs. ** $P < 0.001$, * $P < 0.005$, compared with Scr siRNA control.

Accepted Manuscript

Figure 5. NRP-1 regulated PDGFR mediated MSC migration and proliferation

The effects of NRP-1 knockdown on PDGFR mediated migration and proliferation was investigated. **(A)** Following siRNA knockdown with either scrambled (Scr) control or target NRP-1 siRNAs, the effects on PDGFR mediated migration were determined by exposing MSCs to 20 ng/ml PDGF-AA, PDGF-BB or VEGF-A₁₆₅ in the lower half of a Boyden chamber for 5 h. Dashed line represents level of un-stimulated MSC migration. Data shown are the mean number of migratory cells \pm SD determined from ten random fields from each of three independent experiments. ** $P < 0.001$, * $P < 0.005$, compared with Scr siRNA control. **(B)** Representative images of migratory cells/field (using a 10 \times objective lens) on the membrane underside of a Boyden chamber after 5 h. Basal denotes un-stimulated MSC migration. Ligand-stimulated MSC migration induced by 20 ng/ml PDGF-AA (AA), PDGF-BB (BB) or VEGF-A₁₆₅ (VEGF) in the absence (-) or presence (+) of 100 nM VEGFR2 tyrosine kinase inhibitor (RTK). **(C,D)** Following siRNA knockdown with either Scr control or target NRP-1 siRNAs, the effects on PDGFR mediated proliferation were determined by culturing MSCs for 5 days in either growth medium alone, or growth medium supplemented with **(C)** 10 ng/ml PDGF-AA **(D)** 10 ng/ml PDGF-BB. Data shown are the mean cell number \pm SD determined from triplicate assays from each of two independent experiments, using two different NRP-1 siRNAs. ** $P < 0.001$, * $P < 0.005$, compared with the respective Scr siRNA control MSC proliferation.

Figure 6. NRP-1 co-localization with PDGFRs during MSC network assembly

The co-localization of NRP-1 and PDGFRs was examined during the assembly of MSC networks. MSCs were seeded onto Matrigel, then co-localization of NRP-1 with either PDGFR α at site Y754, or PDGFR β at site Y1021, examined by immunofluorescence microscopy. MSCs cultured for **(A)** 2 h, **(C)** 6 h, **(E)** 24 h, showing PDGFR α -Y754 (green) and NRP-1 (red). MSCs cultured for **(B)** 2 h, **(D)** 6 h, **(F)** 24 h, showing PDGFR β -Y1021 (red) and NRP-1 (green). Below each image, the corresponding red and green channels which have similar threshold values and the same particle size range are shown, together with their co-localization represented by the image in yellow. Nuclei are counter-stained with DAPI (blue). Representative images of at least four independent experiments are shown. Scale bars = 20 μ m.

Figure 7. NRP-1 regulated MSC network assembly

The role of NRP-1 in regulating MSC network assembly was evaluated following NRP-1 knockdown. Following siRNA knockdown with either scrambled (Scr ↓) control or target NRP-1 (NRP ↓) siRNAs, MSCs were seeded onto Matrigel and cultured for 24 h, then co-localization of NRP-1 with either phosphorylated PDGFR α at site Y754, or PDGFR β at site Y1021, examined by immunofluorescence microscopy. Control knockdown MSCs, showing (A) PDGFR α -Y754 (green) and NRP-1 (red), (C) PDGFR β -Y1021 (red) and NRP-1 (green). NRP-1 knockdown MSCs, showing (B) PDGFR α -Y754 (green) and NRP-1 (red). (D) PDGFR β -Y1021 (red) and NRP-1 (green). Nuclei are counter-stained with DAPI (blue). For each image, the corresponding red and green channels having similar threshold values and the same particle size range are shown, together with their co-localization represented by the image in yellow. Wider field images of control knockdown (E) and NRP-1 knockdown MSCs (F) showing PDGFR α -Y754 (green) and NRP-1 (red). Representative images of at least four independent experiments are shown. (G) Bar graph representing the number of branch points per field at 24 h following Scr or target NRP-1 knockdown. Data shown are the mean number of branch points \pm SD determined from at least six random fields from each of four independent experiments, ** P < 0.001, compared with the corresponding Scr siRNA control. Scale bars = 20 μ m.

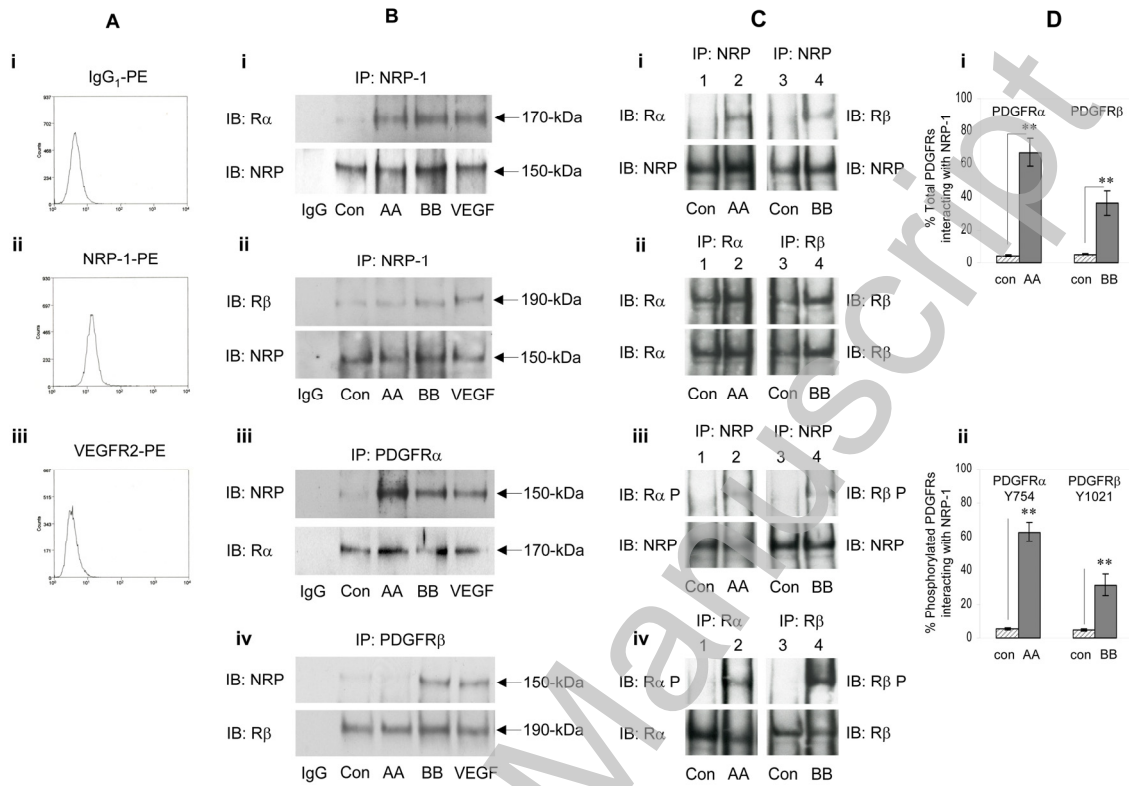
Accepted Manuscript

Figure 8. NRP-1 is essential for *in vivo* MSC networks

The effects of NRP-1 knockdown on MSC network formation was examined using an *in vivo* angiogenesis model system, the CAM of the developing chick embryo. Following siRNA knockdown with either Scrambled (Scr ↓) control or target NRP-1 (NRP ↓) siRNAs, MSCs were seeded onto Matrigel and implanted in direct contact with a highly vascularized area of CAM for 24 h, then co-localization of NRP-1 with either phosphorylated PDGFR α at site Y754, or PDGFR β at site Y1021, examined by immunofluorescence microscopy. Control knockdown MSCs, showing (A) PDGFR α -Y754 (green) and NRP-1 (red), (C) PDGFR β -Y1021 (red) and NRP-1 (green). NRP-1 knockdown MSCs, showing (B) PDGFR α -Y754 (green) and NRP-1 (red), (D) PDGFR β -Y1021 (red) and NRP-1 (green). Control knockdown MSCs, showing (E) PDGFR α -Y754 (green) and NRP-1 (red), (F) PDGFR β -Y1021 (red) and NRP-1 (green). For each image, the corresponding red and green channels having similar threshold values and the same particle size range are shown, together with their co-localization represented by the image in yellow. Nuclei are counter-stained with DAPI (blue). Representative images of two independent experiments are shown. Scale bars = 20 μ m.

Accepted Manuscript

Figure 1



THIS IS NOT THE VERSION OF RECORD - see doi:10.1042/BJ20091512

Accepted Manuscript

Figure 2

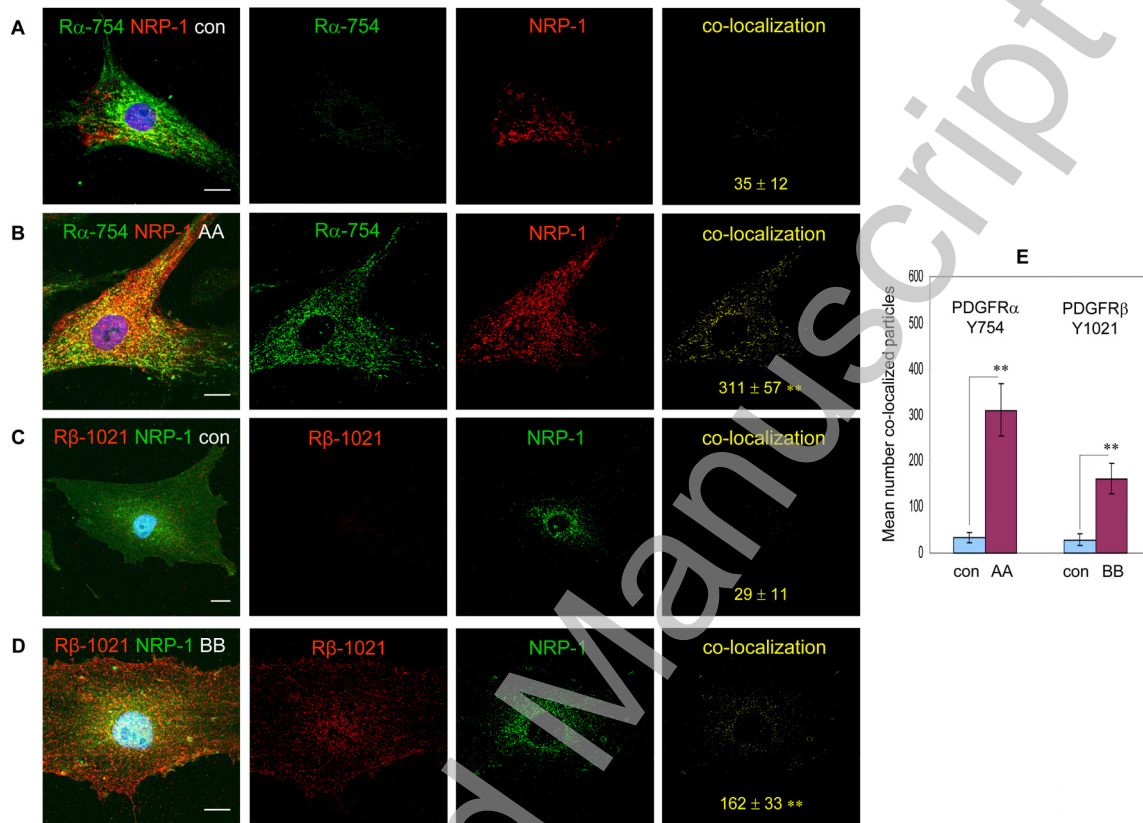
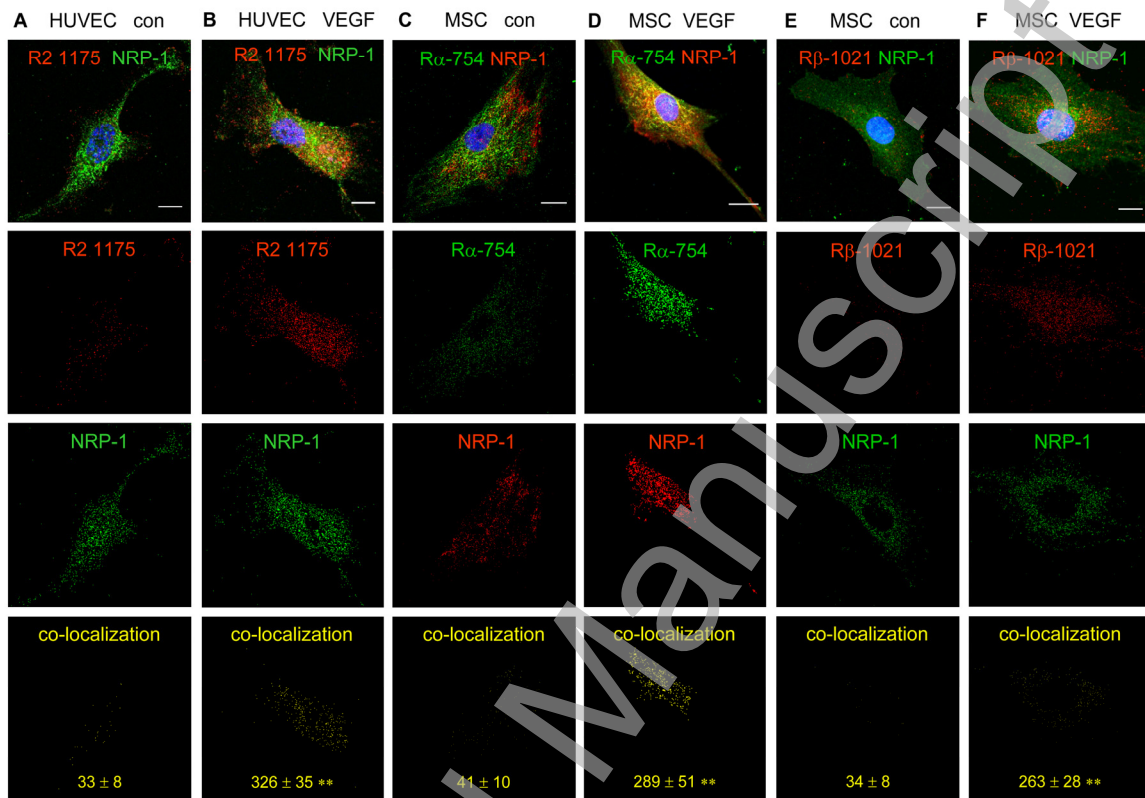


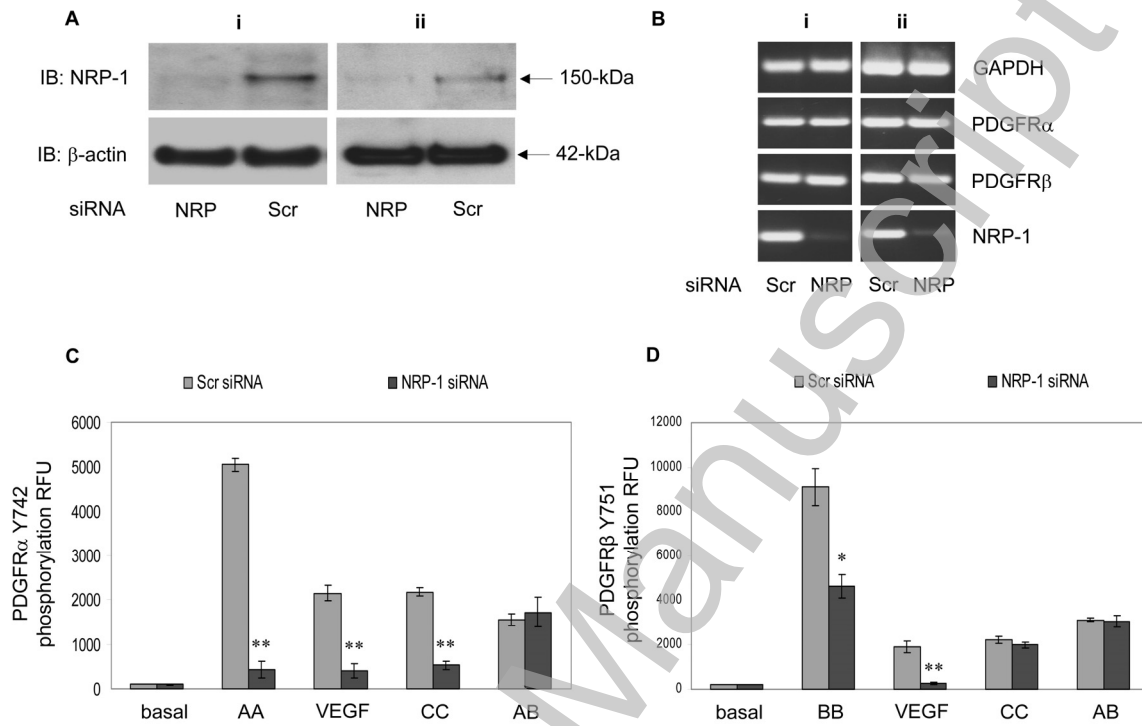
Figure 3



THIS IS NOT THE VERSION OF RECORD - see doi:10.1042/BJ20091512

Accepted Manuscript

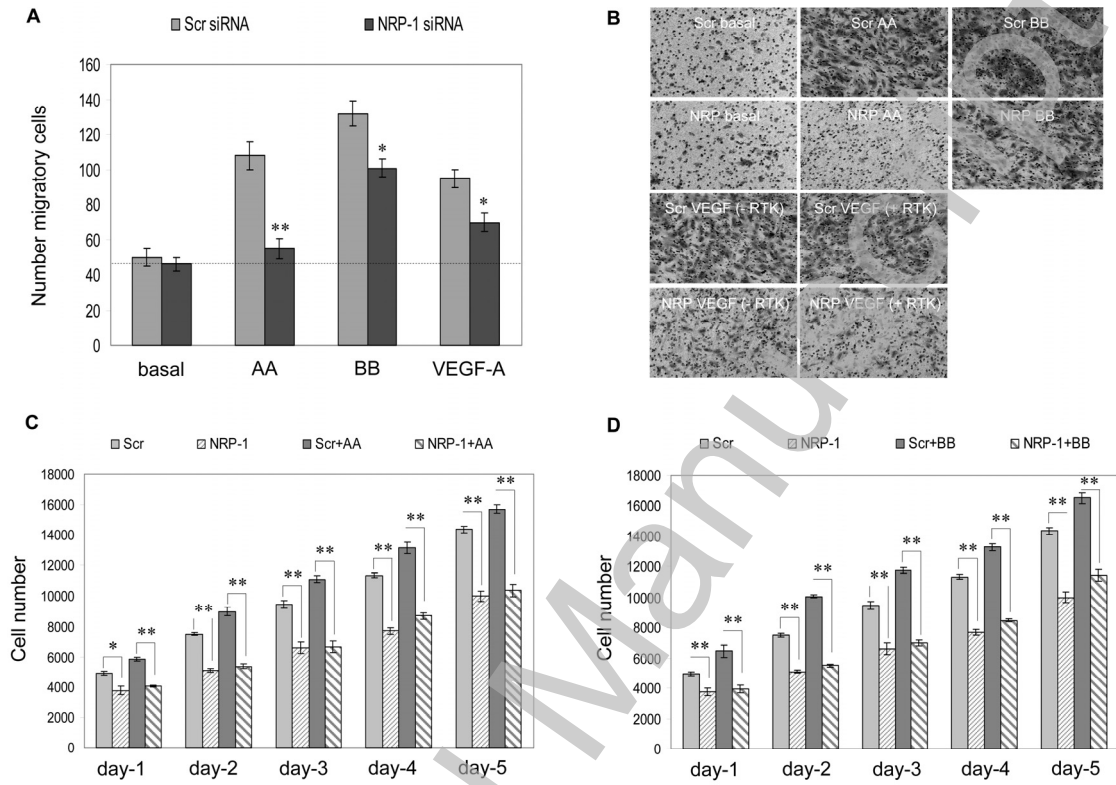
Figure 4



THIS IS NOT THE VERSION OF RECORD - see doi:10.1042/BJ20091512

Accepted Manuscript

Figure 5



THIS IS NOT THE VERSION OF RECORD - see doi:10.1042/BJ20091512

Accepted Manuscript

Figure 6

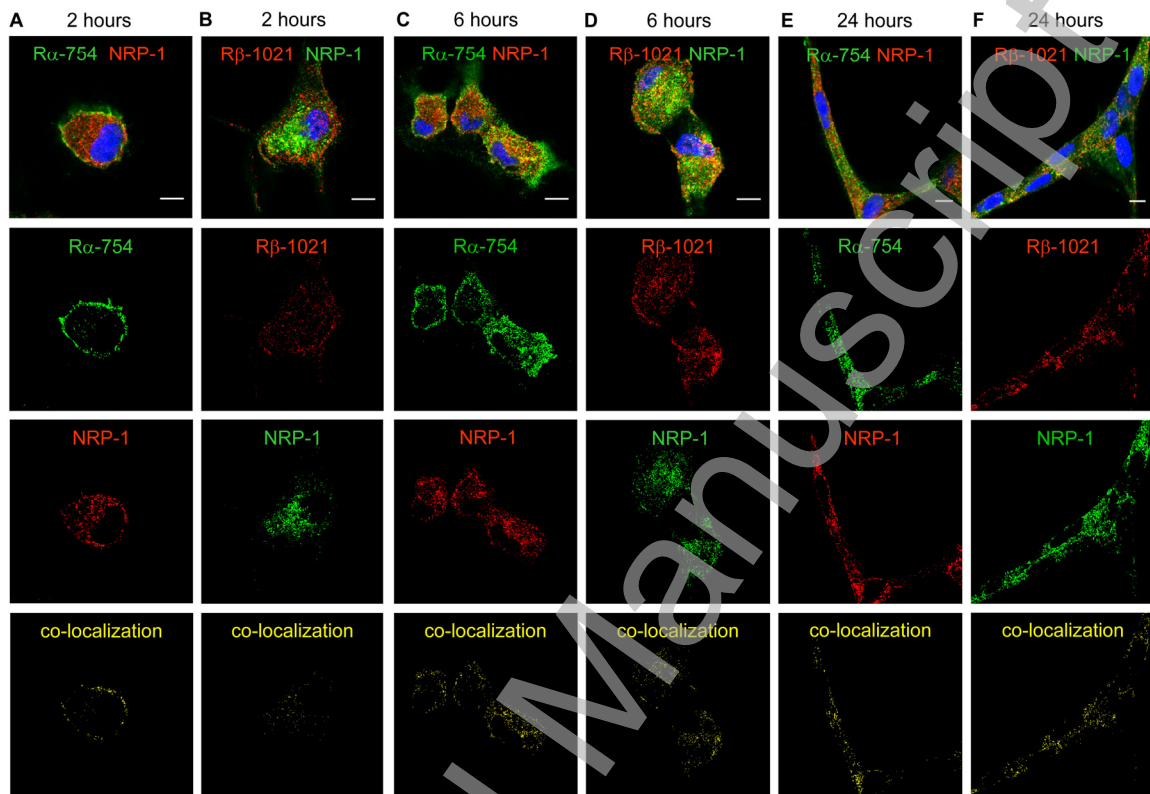
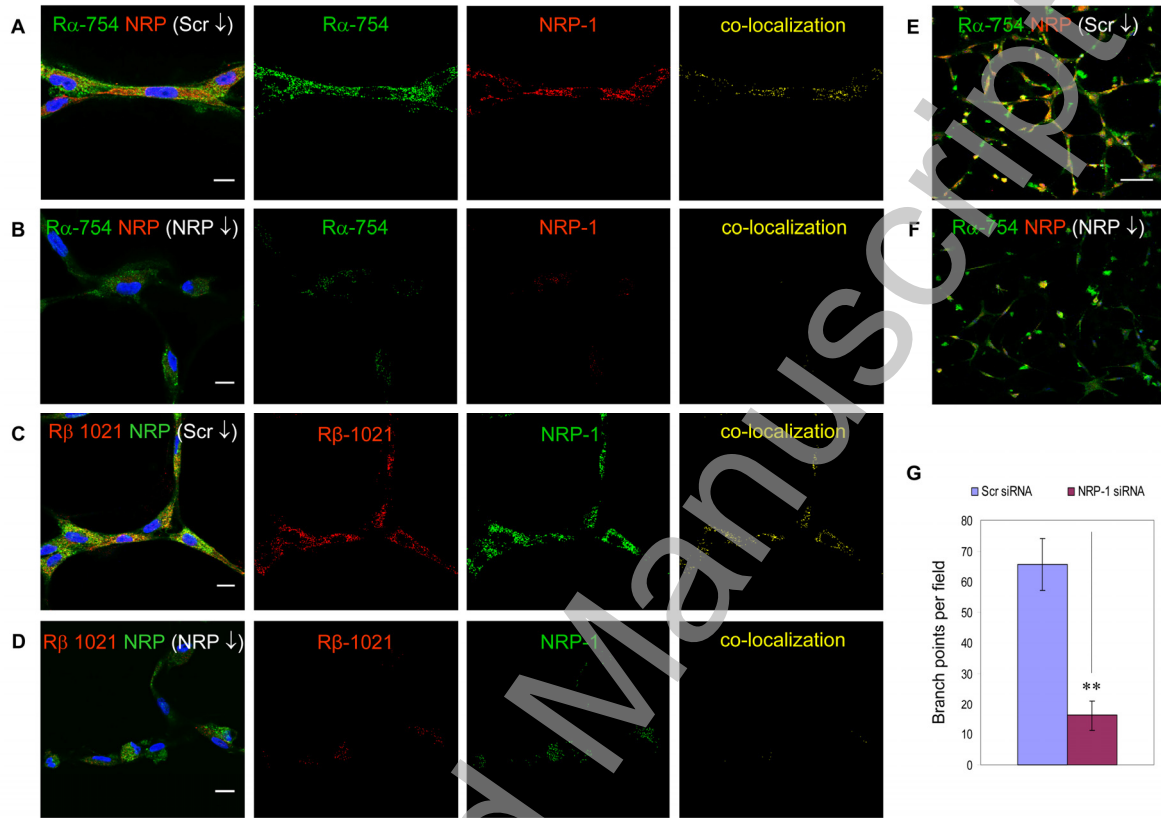


Figure 7



THIS IS NOT THE VERSION OF RECORD - see doi:10.1042/BJ20091512

Accepted Manuscript

Figure 8

